

Hybrid lithium-ion/metal electrodes enable long cycle stability and high energy density of flexible batteries

*Chuan Xie, Jian Chang, Jian Shang, Lei Wang, Yuan Gao, Qiyao Huang, Zijian Zheng**

Dr. C. Xie, Dr. J. Chang, Dr. J. Shang, Dr. L. Wang, Dr. Y. Gao, Dr. Q. Huang, Prof. Z. J. Zheng

Laboratory for Advanced Interfacial Materials and Devices

Institute of Textiles and Clothing

The Hong Kong Polytechnic University

Hong Kong, SAR, China

E-mail: zijian.zheng@polyu.edu.hk

Prof. Z. J. Zheng

Research Institute for Intelligent Wearable Systems (RI-IWEAR)

The Hong Kong Polytechnic University

Hong Kong, SAR, China

Prof. Z. J. Zheng

Research Institute for Smart Energy (RISE)

The Hong Kong Polytechnic University

Hong Kong, SAR, China

Keywords: prelithiation, carbon cloth, flexible battery, cycle stability, hybrid lithium-ion/metal electrode

Abstract

High-energy, stable and flexible lithium batteries are highly demanded for next-generation flexible and wearable electronics. Although the cycling stability of flexible lithium-ion batteries (LIBs) is high, their energy density reaches the bottleneck because of the use of graphite anode. On the other hand, flexible lithium-metal batteries (LMBs) provide higher energy density because of the use of Li metal anode, but the cycling stability is poor. Herein, we report a new type of flexible hybrid lithium-ion/metal battery (f-LIMB), which simultaneously possesses

enhanced energy density, stable cycling behavior, and outstanding flexibility. f-LIMB is enabled by using the prelithiated carbon cloth (preLi-CC) as the anode, which improves the initial Coulombic efficiency (ICE) by a prior formation of solid electrolyte interface (SEI), benefits the subsequent deposition of Li metal due to the preformed lithiophilic Li_xC_6 compounds, and enhances the cycle life and energy density of batteries through a Li compensation mechanism. The f-LIMB full cell possesses an improved gravimetric and volumetric energy density by as much as 64% and 67%, in comparison to the flexible LIB counterpart, and pertains high capacity retention of 84% after 1000 charge/discharge cycles. In addition, the f-LIMB can be readily bent down to a small radius of 2.5 mm.

1. Introduction

With the rapid development of flexible and wearable electronics for a wide variety of applications such as health monitoring^[1], sports and professional training^[2], tracking^[3], robotics^[4], fashion and entertainment^[5], there is an increasing interest in high-performance flexible batteries to replace the conventional rigid type of lithium-ion batteries (LIBs) so as to enable seamless integration between the power supply unit and the other electronic components. To date, much progress has been achieved in the design and fabrication of flexible electrodes, where electrode materials are coated or synthesized on flexible current collectors such as carbon nanotubes and graphene^[6], carbon cloth^[7], and conductive papers/textiles^[8]. This progress has led to the recent demonstrations of numerous flexible pouch cells including flexible LIBs^[9], flexible lithium-metal batteries (LMBs)^[10], flexible dual-ion batteries^[11], and some others^[12]. In particular, several flexible LIBs and LMBs using high-capacity materials such as Si and Li metal have shown high energy density and flexibility^[13].

It should be noted that, in addition to high energy density and flexibility, practical applications also require the battery to retain ~80% of its capacity after 1,000 charge/discharge cycles. To

achieve long-term cycle stability, battery electrodes should reach a high Coulombic efficiency (CE) of over 99.9%^[14]. Despite much effort focused on strategies such as optimization of electrode materials, structures, interfaces, and electrolyte additives, Si and Li metal anodes still suffer severe irreversible active lithium loss (ALL) upon cycling and their CEs are low^[15]. As a result, the majority of these flexible batteries failed after being charged and discharged for 50 to 300 cycles^[13b]. On the other hand, when using high CE electrode such as graphite to improve the cycling stability, the energy density and flexibility of the battery significantly dropped^[13]. To date, how to simultaneously achieve a practically usable cycle life and high energy density of flexible batteries is a challenging topic yet to tackle.

To address this challenge, we report for the first time here a flexible hybrid lithium-ion/metal anode made with prelithiated carbon cloth (preLi-CC), which possesses ultralong cycling stability and high energy density, without sacrificing the flexibility of the battery. The merits of intrinsic conductivity, flexibility, stability, and three-dimensional structure have made carbon cloth (CC) one of the most popular materials for flexible battery applications^[16]. Very recently, several studies on rigid LIBs demonstrated an enhancement of the energy density using hybrid lithium-ion/metal graphite anodes^[17]. In such a hybrid electrode, the cycling stability of Li metal was enhanced by the lithiated graphite^[18]. Nevertheless, the cycling number of these hybrid batteries is still far from satisfactory because of the quick consumption of active lithium caused by the poor reversibility of Li metal. In here, combining the concept of hybrid Li-ion/metal anode and the technique of prelithiation, we constructed the ultra-stable and high-energy flexible lithium batteries. It is known that the prelithiation of LIB anodes provides an extra amount of Li^+ , which compensates for the ALL during charge/discharge^[19]. The prelithiation of CC generates Li_xC_6 in the carbon fibers and minimizes the ALL in the first cycle. Subsequent charging of the preLi-CC forms an additional Li metal layer on the surface of Li_xC_6 to yield the hybrid lithium-ion/metal anode. The preformed Li_xC_6 can act as a ‘backup’ to

compensate for the ALL during cycling and ensure a high CE and long cycling lifetime (**Figure 1**). Therefore, pairing the preLi-CC with commercially available cathodes will yield flexible hybrid lithium-ion/metal batteries (f-LIMBs), which show ultrahigh capacity retention of 84% after 1,000 charge/discharge cycles, improved energy density by ~15%, and excellent electrochemical stability during several hundred bending tests at a small radius of 2.5 mm. Importantly, the preLi-CC demonstrates herein is versatile to pair with essentially any cathode for different kinds of flexible battery applications. More importantly, because the prelithiation is carried out with a simple direct-contact process without any special equipment or assembly of electrochemical cells, it is highly scalable for further industrial usage.

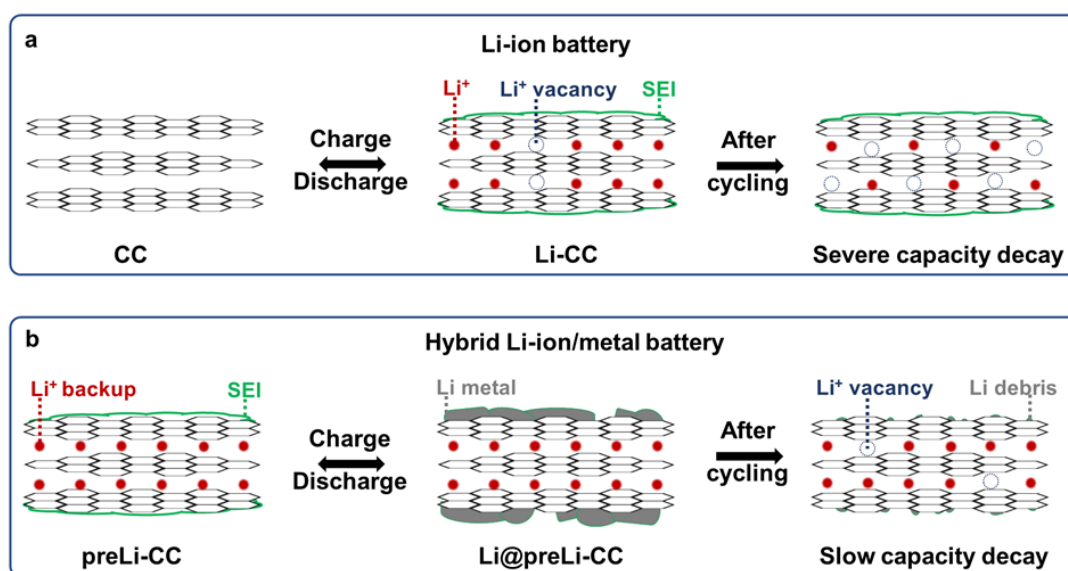


Figure 1. a). Schematic illustration showing the severe active lithium loss and capacity decay in a traditional LIB made with pristine CC. b). Schematic illustration showing the mechanism of hybrid Li-ion/metal battery assembled with preLi-CC.

2. Results and discussion

2.1. Fabrication and characterization of preLi-CC

preLi-CC was fabricated with a facile direct-contact prelithiation method (**Figure 2a**). A piece of commercially available CC was first tightly pressed on top of a Li foil to ensure good contact, and a few drops of electrolyte were then applied to wet the entire CC. Because of the low electrochemical reduction potential of Li metal, the CC was spontaneously lithiated driven by the difference of Gibbs free energy between CC and Li metal^[18a, 20]. The prelithiation process typically took a period ranging from 10 min to overnight, depending on the amount of Li required. After rinsing and drying, the as-prepared preLi-CC was ready for further characterization and use, and the rest of the Li foil was reused for lithiating other samples.

The successful lithiation of CC can be readily evidenced by the morphological change observed under scanning electron microscopy (SEM). The pristine carbon fibers possessed a clean and smooth surface (Figure 2b and 2c). In contrast, the surface of lithiated fibers became rough and was covered with microcracks (Figure 2d and 2e). These cracks are likely to be caused by the volume expansion during the formation of Li_xC_6 compounds upon prelithiation^[18a]. The color of the sample changed from black to deep purple after lithiation (Inset, Figure 2b and 2d).

X-ray diffraction (XRD) analysis showed an obvious downshift of the strong C peak from 25.5° to 24.5° after the prelithiation. This downshift is attributed to the enlarged interlayer spacing as a result of the formation of Li_xC_6 (Figure 2f). We also observed two new peaks at 32.5° and 35.8° , which are respectively attributed to Li_2O or Li_2OH formed by the reaction between Li_xC_6 and moisture in the air^[18a, 21]. X-ray photoelectron spectroscopy (XPS) analysis of preLi-CC showed the emergence of strong broad peaks centered at 55.1 eV, 289.2 eV, and a shoulder peak at 286.5 eV (Figure 2g, 2h, and S1a, S1b). These peaks are typical characteristics of the solid electrolyte interface (SEI) formed during the lithiation process. The compositions of these Li-containing compounds are thought to be LiF, Li_2O , Li_2CO_3 , and organic Li compounds^[22].

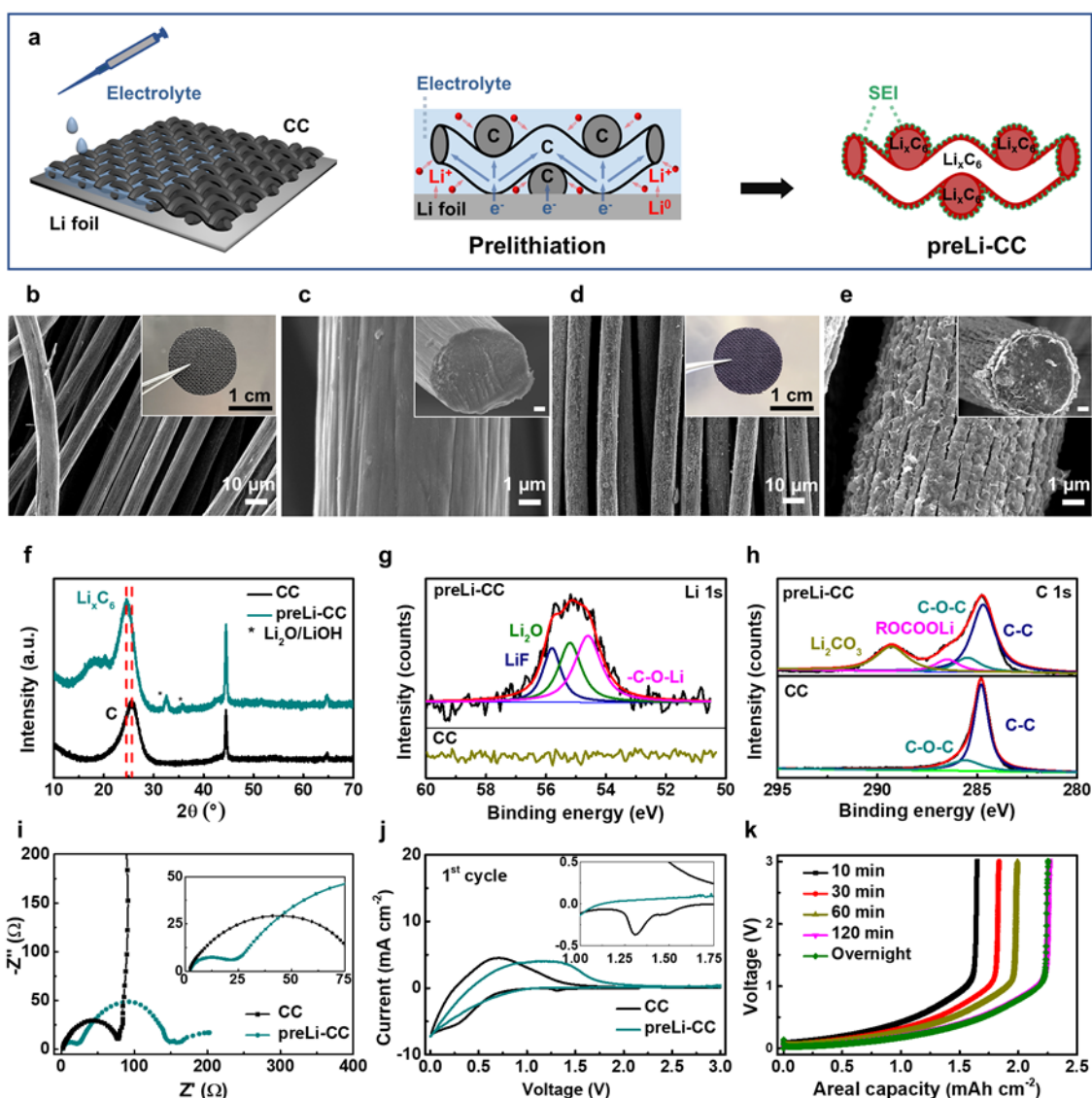


Figure 2. Preparation and characterization of the preLi-CC electrode. a) Schematic illustration of the preparation of preLi-CC electrode by direct-contact prelithiation. b-e) Images of the pristine carbon fiber (b, c), and prelithiated carbon fiber (d,e). The scale bar in the inset is 1 μm . f) X-ray diffraction (XRD) patterns of CC and preLi-CC. g) Li 1s X-ray photoelectron spectroscopy (XPS) spectrum of CC and preLi-CC. h) C 1s XPS spectrum of CC and preLi-CC. i) Electrochemical impedance spectroscopy (EIS) of CC and preLi-CC electrodes upon assembly. j) Cyclic voltammetry (CV) curves of CC and preLi-CC in the 1st cycle at a scan rate of 1 mV s^{-1} in a potential window from 0.001 to 3 V. The inset images indicate the zoomed-in curves from 1 to 1.75 V. k) Capacity of the extracted Li from preLi-CC electrodes treated for different time. The current density is 0.25 mA cm^{-2} .

The formation of SEI during prelithiation can be also evidenced by electrochemical impedance spectroscopy (EIS) and cyclic voltammetry (CV) scans of the electrodes countered with Li foil. For the pristine CC, only one semi-circle representing the charge transfer resistance was observed in the EIS analysis before the CV scan (Figure 2i). In the first cycle of the CV scan, a strong reduction peak at ~ 1.25 V appeared as a result of the formation of SEI as analyzed in the literature^[22a] (Figure 2j and S1c). A second semi-circle belonging to the SEI resistance emerged in the subsequent EIS test, which is also an indication of the formation of SEI^[23] (Figure S1d). In contrast, both semi-circles already existed in the first EIS test of the preLi-CC before the CV scan, and no reduction peak was observed at the first CV scan of the preLi-CC. Both results indicated that the SEI was already formed in preLi-CC during the prelithiation process. The energy dispersive x-ray (EDX) mapping showed uniform distribution of O and F on the carbon fiber of the preLi-CC anode after stripping the Li^+ away, demonstrating the uniformity of SEI on the surface (Figure S2).

We quantified the amount of capacity by fully extracting the intercalated Li^+ out of preLi-CC. We found that the direct-contact prelithiation process was very quick and efficient: 1.65 mAh cm^{-2} of Li^+ was stored in the carbon fibers in only 10 minutes. The capacity increased to 1.84, 1.99, and 2.27 mAh cm^{-2} when the prelithiation time was lengthened to 30, 60, and 120 minutes, respectively. Further treating the CC overnight did not increase the capacity because the carbon fibers were fully lithiated (Figure 2k). Other advantages of the direct-contact prelithiation method include the low materials costs, low requirement of equipment, low reduction potential of Li metal, and high capacity of lithiation among the reported prelithiation methods as has been discussed in several review literature^[17]. A large scale of samples can easily be fabricated through this method. The fully lithiated preLi-CC is used as the anode for the further construction of hybrid lithium-ion/metal batteries.

2.2. Electrochemical behavior of preLi-CC as hybrid Li-ion/metal anode

We assembled the CC and preLi-CC electrodes with Li metal counter electrode to study their electrochemical behaviors. A total capacity of 2 mAh cm^{-2} of Li was discharged onto the CC or preLi-CC electrode and then stripped out. Before discharge, the fresh CC//Li cell showed an open-circuit voltage of $\sim 2 \text{ V}$. The discharge process of CC showed two typical stages including the formation of SEI and the intercalation of Li^+ (Figure 3a). The small plateau at $\sim 1.25 \text{ V}$ (Figure 3a inset) reflects the decomposition of Li salts and solvents, and the formation of SEI, which is in agreement with the CV tests discussed above. When reversing the electric field to charge, the Li^+ were completely deintercalated with the voltage increasing to 2 V . Because of the partial consumption of the Li source during the SEI formation, the ICE was only 91.20%. We observed the intercalation and deintercalation of Li^+ when the cell was cycled (Figure S3a). The CE increased to 99.90% after 10 charge/discharge cycles (Figure 3b). The CC electrode shows a typical LIB anode behavior similar to that of the graphite anode.

The preLi-CC electrode showed completely different behavior. There was no sign of the SEI formation or intercalation (Figure 3c). The open-circuit voltage of the preLi-CC//Li cell was 10 mV before discharge. After discharge, all 2 mAh cm^{-2} was deposited on the preLi-CC surface in the form of Li metal. Upon charge, the deposited Li metal was stripped out completely and the ICE reached 100.00%. We observed a small voltage increase of 35 mV at the end of the charging process, indicating that a very small portion of the prestored Li^+ (estimated to be 0.2 mAh cm^{-2} from the voltage profile) in the preLi-CC was stripped out to compensate for the capacity loss of the Li metal, which might be consumed by side reaction or dead Li. The average CE maintains very stably over 99.99% for over 200 cycles (Figure 3b). We also observed that because of the small consumption of the prestored Li^+ in each cycle, the ratio between the Li metal to Li^+ in one charge gradually decreased. This can be evidenced by the increasing termination voltage of each charge cycle of the voltage profile (Figure S3b). And increasing the

current density to 2 mA cm^{-2} did not lead to performance degradation of the preLi-CC anode (Figure S3c). Because the charging process consisted of both stripping of Li metal and Li^+ , the electrode is considered a hybrid Li-ion/metal anode.

The indispensable role of preformed Li_xC_6 can be confirmed by comparing samples with different pretreatment methods (Figure 3d). After stripping the preformed Li_xC_6 before cycling (S-preLi-CC), the average CE in 50 cycles was only 99.89%, similar to the CE of activated CC (99.87%) and higher than that of the pristine CC (99.68%). Without the preformed Li_xC_6 to supply active lithium during cycling, none of the anodes provides comparable CE as the preLi-CC. Notably, a 100% CE was also obtained when the electrochemically prelithiated EpreLi-CC was used. An identical hybrid Li-ion/metal storage behavior was observed due to the presence of Li_xC_6 similar to the preLi-CC prepared by the direct-contact method (Figure S4), demonstrating the important role of preformed Li_xC_6 as ‘backup’ lithium (through either direct-contact prelithiation or electrochemically prelithiation). Besides, the electrolyte had a significant influence on the stability of the preLi-CC anode. The preLi-CC anode showed a quick drop of CE when LiPF_6 -based electrolyte was used for cell assembly because of the poor compatibility with Li metal^[17b, 17d]. The influence of electrolyte used for the prelithiation, on the other hand, is only marginal when comparing the intercalated capacity and CE (Figure S5), though SEI components displayed much difference after prelithiation (Figure S6). Further studies are expected to be carried out in the future to thoroughly investigate the formation of SEI during the process of direct-contact prelithiation and electrochemically reduction.

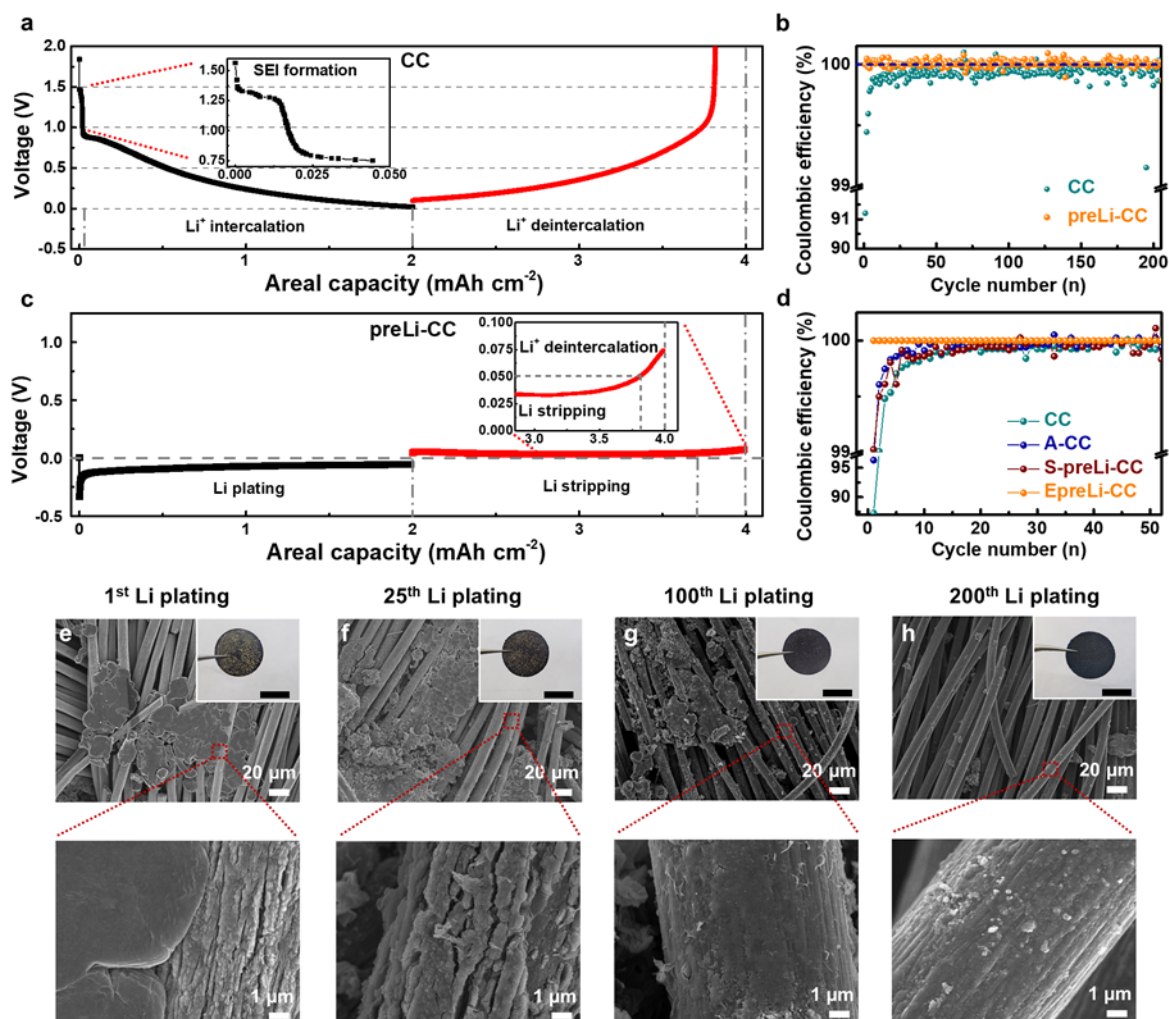


Figure 3. Electrochemical behavior of CC and preLi-CC electrodes. a) The first charge/discharge curves of the CC//Li cell. The inset image is the zoomed-in curve from 0 to 0.05 V. b) CEs of pristine CC and preLi-CC anode. The current density was 1 mA cm⁻². c) The first charge/discharge curves of the preLi-CC//Li cell under the same condition as the CC electrode. The inset image is the zoomed-in curve from 2.8-4.1 V. d) CEs of the pristine CC, activated CC (A-CC), stripped preLi-CC, and electrochemically prelithiated CC (E-preLi-CC) anode. The current density used here was 2 mA cm⁻². e-h). Images of the preLi-CC after 1st (e), 25th (f), 100th (g), and 200th Li deposition (h). Inset. Digital images of the electrodes after Li deposition (scale bar, 1 cm).

From SEM observation, we also found a gradual loss of Li metal in our hybrid anode. The surface of the preLi-CC electrode was well covered by Li metal (Figure 3e). The coverage of Li metal decreased as the cell was cycled to the 25th and 100th cycles (Figure 3f and 3g). After

200 cycles, little Li metal was observed on the fiber surface (Figure 3h). As expected, the deposited Li metal vanished after each stripping cycle (Figure S7). Importantly, little Li dendrite or dead Li was observed during the entire cycling process, showing the remarkable stability of the anode. As a comparison, no Li metal forms during the entire charge/discharge process for the CC electrode. The CC transformed into lithiated CC (Li-CC) during Li^+ intercalation and change back to CC after stripping the Li^+ away. And the growth and disappearance of Li_xC_6 can be reflected by the morphological change of the carbon fiber (Figure S8).

2.3. Flexible hybrid Li-ion/metal batteries (f-LIMBs)

The f-LIMBs can be fabricated by pairing the Li-containing cathode (e.g., LiFePO_4 and LiCoO_2) with the preLi-CC anode. The working principle of the f-LIMB is illustrated in **Figure 4a**. The active Li from the cathode deposits on the preLi-CC in the form of Li metal during the charging process. The prestored Li^+ in the anode compensates for the ALL during long-term cycling. Because the amount of active Li in a full cell is limited by the cathode side, the f-LIMBs are expected to possess higher energy density and longer cycle life than the flexible LIBs made of the same cathodes. In addition, because the prelithiation process does not affect the flexibility of the anode, the hybrid batteries should pertain high flexibility.

As a proof of concept, we fabricated f-LIMBs based on the configuration of LFP//preLi-CC and studied the detailed electrochemical characteristics against its reference cell LFP//CC. In the first charge process, both cells showed a capacity of $\sim 2.05 \text{ mAh cm}^{-2}$ at 0.5 C, which was consistent with the areal capacity of the commercial LFP cathode (Figure 4b). In the subsequent first discharge process, the LFP//CC showed a low ICE of 88.86% and an ALL of 0.23 mAh cm^{-2} due to the SEI formation and irreversible side reactions on CC, while the ICE of the LFP//preLi-CC could be increased to 93.04% thanks to the preformed SEI and suppressed side

reactions. Therefore, the first discharge capacity of the LFP//preLi-CC (1.91 mAh cm^{-2}) was much higher than that of the LFP//CC (1.82 mAh cm^{-2}).

The CE of the LFP//preLi-CC increased to over 99.72% immediately after the first cycle and maintained stably at $\sim 99.95\%$ after 10 cycles. In contrast, the CE of the LFP//CC in the first 10 cycles was low and slowly increased to 99.90% after 10 cycles. The average CE of the LFP//CC was only 99.86%. As a consequence of the different CE, the LFP//preLi-CC showed much better cycling stability with a capacity retention of 84% (from 1.91 to 1.60 mAh cm^{-2}) after 1000 cycles, whereas the capacity retention of the LFP//CC was only 60% (from 1.82 to 1.10 mAh cm^{-2}). On the other hand, when using Li foil as the anode, an LMB behavior was presented with a discharge voltage plateau of 3.38 V. However, the capacity decayed quickly after only 134 cycles because of the issues of electrolyte dry out and Li dendrites growth (Figure S9).

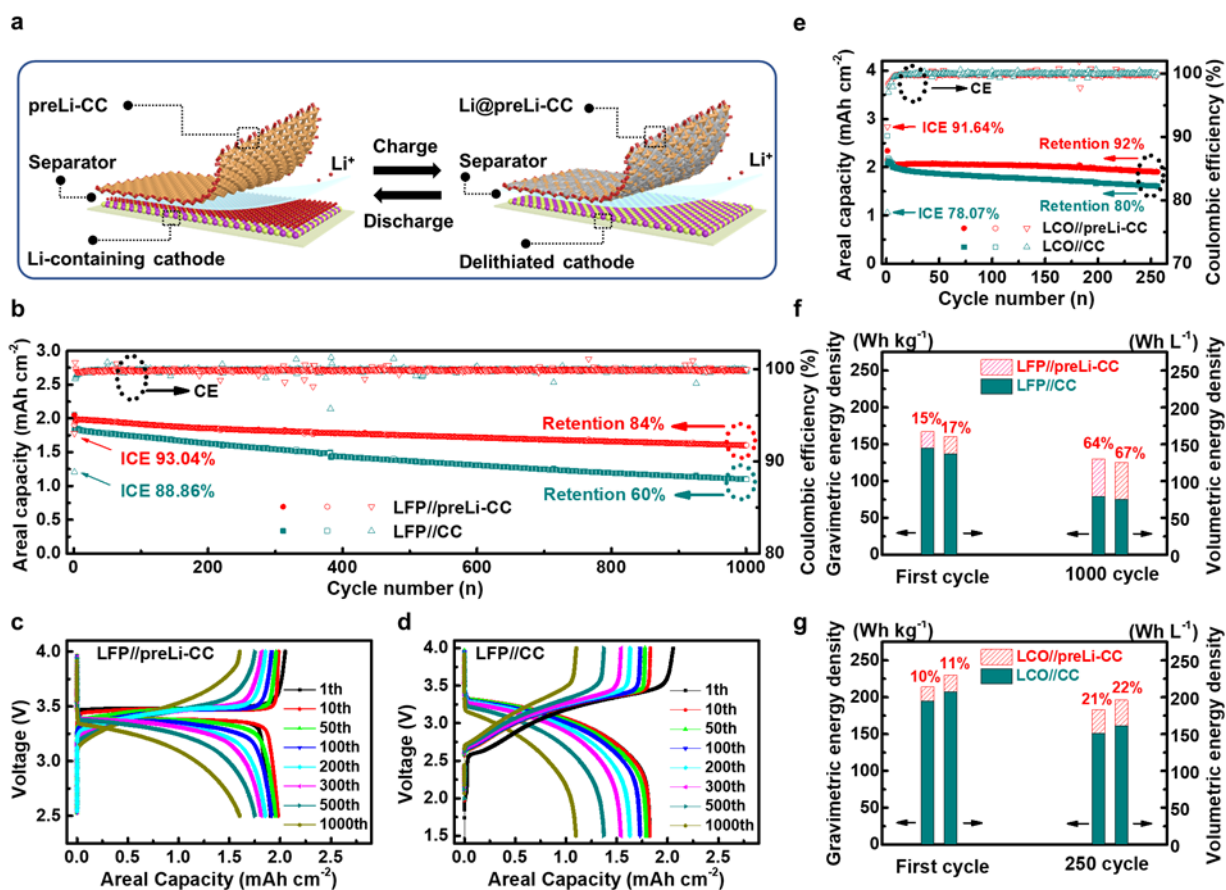


Figure 4. Full-cell performances of the CC and preLi-CC anodes paired with LFP and LCO cathodes. a) The working mechanism of the flexible hybrid lithium-ion/metal batteries (f-LIMBs. b) Cycling stability of the LFP//preLi-CC and LFP//CC. The cells were tested at a current density of 1 mA cm^{-2} from 2.5-4 V for LFP//preLi-CC and 1.5-4 V for LFP//CC. c) Charge/discharge profiles of the LFP//preLi-CC. d) Charge/discharge profiles of the LFP//CC. e) Cycling stability of the LCO//preLi-CC and LCO//CC batteries using carbonate electrolyte. The cells were tested at a current density of 0.5 mA cm^{-2} from 3-4.3 V for LCO//preLi-CC and 2.5-4.3 V for LCO//CC. f-g) Comparison of the gravimetric and volumetric energy densities of the LFP//preLi-CC and LFP//CC (f), and LCO//preLi-CC and LCO//CC (g) in the first and last cycles.

Apart from a larger first cycle capacity and better cycle stability, the LFP//preLi-CC also possessed a higher discharge voltage than the LFP//CC. The LFP//preLi-CC showed a stable discharge plateau at 3.38 V in the first cycle, with only 100 mV of voltage hysteresis (Figure 4c), indicating an LMB behavior. The discharge plateau then gradually shortened and finally disappeared after a few hundred cycles, indicating the gradual conversion from the LMB to LIB behavior. In contrast, the discharge voltage profile of the first cycle of the LFP//CC displayed an obvious slope decreasing gradually from 3.38 V to 2.40 V (Figure 4d), indicating a pure LIB behavior. The midpoint discharge voltage was 3.10 V at the first cycle and then significantly reduced to 2.82 V.

We observed similar advantages of the LCO//preLi-CC over LCO//CC using commercial carbonate electrolyte. As shown in Figure 4e, the LCO//preLi-CC run stably for more than 250 cycles with a high ICE of 92% and capacity retention of 92% (from 2.06 to 1.91 mAh cm^{-2}). The midpoint discharge voltage of the LCO//preLi-CC was ~ 3.90 V at the first cycle and dropped to 3.76 V after 250 cycles (Figure S10a). In contrast, the LCO//CC presented a low ICE of 78.07% and capacity retention of 80% (from 2.01 to 1.61 mAh cm^{-2}). The midpoint

discharge voltage of the LCO//CC was only ~ 3.70 V at the first cycle and dropped to 3.68 V after 250 cycles (Figure S10b).

Benefitting from the larger initial capacity, higher midpoint voltage, and better average CEs, the energy density of f-LIMB is much higher than their LIB counterparts. In our experiments, the gravimetric and volumetric energy density of the LFP//preLi-CC were 167 Wh kg^{-1} and 160 Wh L^{-1} , respectively (Figure 4f). These equal to a remarkable increment of 15% and 17% of energy density in comparison to the LFP//CC. The difference of energy density was more prominent after cycling. The LFP//preLi-CC presented an improved gravimetric and volumetric energy density by as much as 64% and 67%, respectively, over that of the LFP//CC after 1000 cycles. Similarly, the energy density reached 214 Wh kg^{-1} and 230 Wh L^{-1} for the LCO//preLi-CC battery with enhancement by 10% and 11% respectively compared with the LCO//CC battery. The LCO//preLi-CC battery presented an improved gravimetric and volumetric energy density by 21% and 22%, respectively, over that of the LCO//CC after 1000 cycles (Figure 4g).

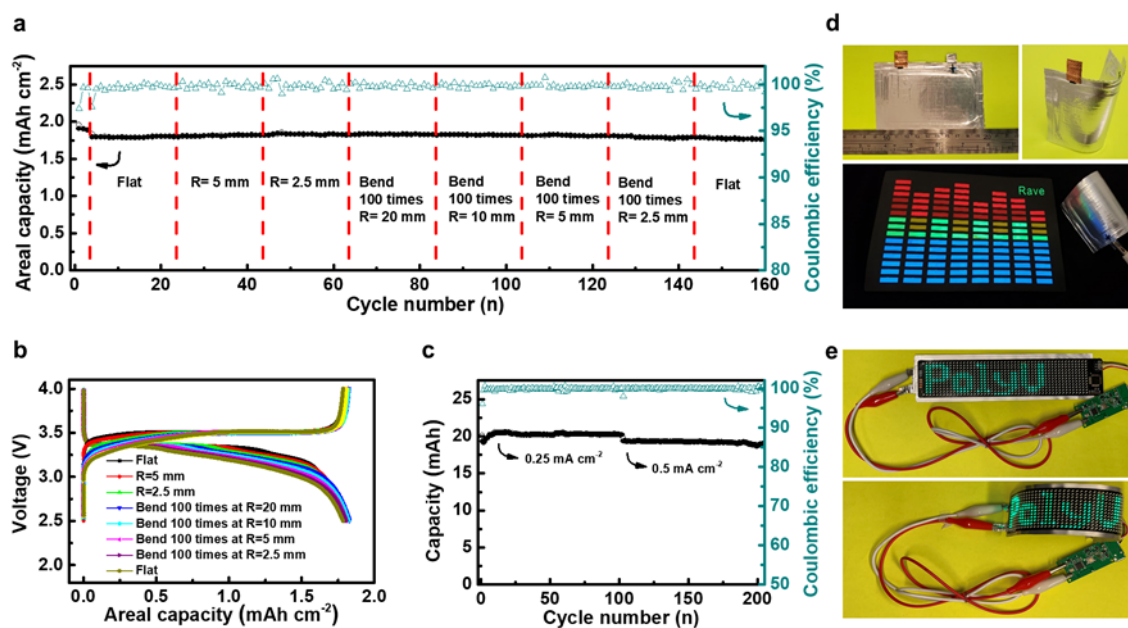


Figure 5. Flexibility test of the preLi-CC-based batteries. a) Flexibility performance of the

LFP//preLi-CC pouch cell. The cell was tested at a current density of 0.5 mA cm^{-2} from 2.5-4 V. b) Charge/discharge curves of the LFP//preLi-CC pouch cell under different bending states. c) Long-time cycling test of the LFP//preLi-CC pouch cell. d) Images showing a large flexible pouch cell with the size of $5 \times 8 \text{ cm}^2$ under a flat and bent state. And the flexible pouch cell successfully lighted a LED T-shirt under a curved state. e) Images showing a flexible LED panel lit by a flexible pouch cell under a flat and bent state when attached together.

The high flexibility of the LFP//preLi-CC ($2.5 \text{ cm} \times 4 \text{ cm}$ pouch cell) was demonstrated by bending the battery at different radii of curvatures from 20 mm to 2.5 mm (**Figure 5a**). The cell was firstly cycled at a bent state under a bending radius of 5 mm or 2.5 mm. The capacity showed little change. We then bent the cell 100 times each at different radii decreasing from 20 mm, 10 mm, 5 mm, to 2.5 mm. Notably, the capacity maintained high stability, and no obvious capacity drop or cell failure was observed. The capacity retention was 97.8% (from 1.82 mAh cm^{-2} to 1.78 mAh cm^{-2}) after those bending tests. The charge/discharge profiles at different bending states showed the flat discharge plateaus at 3.38 V at the beginning and the flat plateaus gradually transform into sloping curves (**Figure 5b**), which are in accord with the profiles of unbent cells. As shown in **Figure 5c**, the large-size pouch cell showed almost zero capacity degradation after running for 200 cycles. **Figure 5d** presents a large LCO//preLi-CC pouch cell ($5 \text{ cm} \times 8 \text{ cm}$) with a total capacity of $\sim 100 \text{ mAh}$. This LCO//preLi-CC could readily power a wearable LED T-shirt when it was sewn on the fabric. **Figure 5e** shows a flexible LED panel was successfully lit by a flexible LCO//preLi-CC pouch cell under a flat and bent state when they were attached together. Compared with the state-of-the-art flexible lithium batteries, our work is the only reported flexible battery that maintained over 80% of capacity after 1000 cycles (**Table S1**). The flexibility and energy density of the f-LIMB is also good among these works. The excellent flexibility and high energy density of the f-LIMBs show great application potential in the field of flexible and wearable electronics.

3. Conclusions

In summary, we prepared the flexible and stable hybrid lithium-ion/metal anode by a facile direct contact prelithiation method, and demonstrated the superior electrochemical stability and excellent flexibility of the f-LIMBs. The prelithiation process can eliminate ALL caused by SEI formation and side reactions, introduce extra Li^+ into the anode, and ease the subsequent deposition of Li metal. In comparison to flexible LIBs, f-LIMBs showed a much enhanced initial CE, higher midpoint discharge voltage, higher energy density, and higher capacity retention (84% after 1000 cycles). Importantly, the preLi-CC was compatible with the commercial carbonate electrolyte and high-capacity LCO cathodes. The flexibility of the f-LIMBs was also demonstrated using large-area pouch cells. The good electrochemical performance of the cell was well retained even when bent at a small radius of 2.5 mm for hundreds of times. The combination of the prelithiation technique and the novel concept of f-LIMBs provides a new strategy for the design and manufacture of future high-energy flexible lithium batteries.

4. Methods

Materials and characterization.

All chemicals and materials are used as received unless otherwise specified. The LFP and LCO cathodes are received from the Southern University of Science and Technology (SUSTech) and dried at 120 °C overnight under high vacuum before use. The LiTFSI-based electrolyte is prepared by dissolving 1 M lithium bis(trifluoromethanesulfonyl)imide (LiTFSI) in 1,3-dioxolane (DOL) and 1,2-dimethoxyethane (DME) (1:1 in volume) with 2 wt.% LiNO_3 . The LiPF_6 -based electrolyte is commercially available from Sigma-Aldrich with 1M LiPF_6 dissolved in ethylene carbonate (EC)/ ethylmethyl carbonate (EMC)/ dimethyl carbonate (DMC) (1:1:1 in volume) as solvent.

The morphological measurements of the electrodes were carried out in a field emission

scanning electron microscopy (FESEM, JSM6335F, JEOL, Japan).

The X-ray diffraction (XRD) tests were performed on a Bruker D8 Avance diffractometer equipped with a Cu-K α radiation source.

The surface compositions of carbon fibers were characterized by X-ray photoelectron spectroscopy (XPS) with an Al-K α excitation source.

Cyclic voltammetry (CV) and electrochemical impedance spectroscopy (EIS) tests were performed on a CHI660e electrochemical workstation. The CV was tested at a voltage window of 0-3 V under a sweeping voltage of 1 mV S⁻¹. The scanning of EIS was tested with an amplitude voltage of 10mV in a frequency range from 100 kHz to 50 mHz.

Preparation of preLi-CC.

The preLi-CC was prepared by pressing a piece of CC and Li foil together tightly and dropping several drops of LiTFSI-based electrolyte to wet the CC. The CC and Li were sealed with aluminum laminate composite foil to prevent the electrode from contamination. After a certain period, the electrode was peeled off and rinsed with DME three times, and the electrode was dried at room temperature before use. The whole process was performed in an Ar-filled glovebox (O₂, H₂O < 1 ppm).

The preLi-CC prepared with LiPF₆-based electrolyte was fabricated with the same method except the electrolyte was changed.

The electrochemically prelithiated CC (EpreLi-CC) was prepared through electrodeposition. The CC was assembled into a coin cell using Li foil as the counter electrode and LiTFSI-based electrolyte. The lithiation of CC was controlled through electrochemically discharging the cell to 0 V at a small current density of 0.25 mA cm⁻². The EpreLi-CC was obtained after disassembling the coin cell and washing with DME three times.

Electrochemical measurement.

All the batteries were assembled in an Ar-filled glovebox with oxygen and water < 1ppm. For the half cell, the electrodes were punched into 1.6 cm-diameter circular electrodes and

celgard-2032 membranes were used as the separator, and 500 μm Li foils were used as both counter and reference electrode with 80 μL LiTFSI-based electrolyte. For the LFP full cell, the LFP was used as the cathode, and CC or preLi-CC were used as anodes with 80 μL LiTFSI-based electrolyte. The LiPF_6 -based electrolyte (1M LiPF_6 in EC/EMC/DMC, 1:1:1 in volume) was used for LCO full cell. For the pouch cell assembly, the aluminum laminate composite foil was used to seal the cell with 20 $\mu\text{L cm}^{-2}$ electrolyte added. All the galvanostatic tests were done by the Neware battery testing system (BTS-4008, Shenzhen, China).

Supporting Information

Supporting Information is available from the Wiley Online Library or from the author.

Acknowledgements

The authors acknowledge financial support from the Shenzhen Municipal Science and Technology Innovation Commission (SGDX20190816232209446) and Research Talent Hub for Innovation and Technology Fund (PRP/055/21FX). The authors also thank Professor Yonghong Deng from the Southern University of Science and Technology and CAPCHEM for providing the LFP, LCO, and other materials for experiments.

Conflict of Interest

The authors declare no conflict of interest.

Received: ((will be filled in by the editorial staff))

Revised: ((will be filled in by the editorial staff))

Published online: ((will be filled in by the editorial staff))

Reference

- [1] a) T. R. Ray, J. Choi, A. J. Bandodkar, S. Krishnan, P. Gutruf, L. Tian, R. Ghaffari, J. A. Rogers, *Chem. Rev.* **2019**, 119, 5461; b) X. Tian, P. M. Lee, Y. J. Tan, T. L. Y. Wu, H. Yao, M. Zhang, Z. Li, K. A. Ng, B. C. K. Tee, J. S. Ho, *Nature Electronics* **2019**, 2, 243.
- [2] Y. Yang, W. Gao, *Chem. Soc. Rev.* **2019**, 48, 1465.
- [3] Q. Shi, Z. Zhang, T. He, Z. Sun, B. Wang, Y. Feng, X. Shan, B. Salam, C. Lee, *Nat. Commun.* **2020**, 11, 4609.
- [4] A. Chortos, J. Liu, Z. Bao, *Nat. Mater.* **2016**, 15, 937.
- [5] a) X. Shi, Y. Zuo, P. Zhai, J. Shen, Y. Yang, Z. Gao, M. Liao, J. Wu, J. Wang, X. Xu, Q. Tong, B. Zhang, B. Wang, X. Sun, L. Zhang, Q. Pei, D. Jin, P. Chen, H. Peng, *Nature* **2021**, 591, 240; b) D. Wang, Y. Zhang, X. Lu, Z. Ma, C. Xie, Z. Zheng, *Chem. Soc. Rev.* **2018**, 47, 4611.
- [6] a) L. Hu, H. Wu, F. La Mantia, Y. Yang, Y. Cui, *ACS Nano* **2010**, 4, 5843; b) N. Li, Z. Chen, W. Ren, F. Li, H. M. Cheng, *Proc. Natl. Acad. Sci. U. S. A.* **2012**, 109, 17360.
- [7] a) B. Liu, J. Zhang, X. Wang, G. Chen, D. Chen, C. Zhou, G. Shen, *Nano Lett.* **2012**, 12, 3005; b) S. H. Ha, K. H. Shin, H. W. Park, Y. J. Lee, *Small* **2018**, 14, 1703418.
- [8] a) Y. H. Lee, J. S. Kim, J. Noh, I. Lee, H. J. Kim, S. Choi, J. Seo, S. Jeon, T. S. Kim, J. Y. Lee, J. W. Choi, *Nano Lett.* **2013**, 13, 5753; b) K. Lee, J. H. Choi, H. M. Lee, K. J. Kim, J. W. Choi, *Small* **2018**, 14, e1703028; c) Y. Gao, C. Xie, Z. Zheng, *Adv. Energy Mater.* **2020**, 11, 2002838.
- [9] W. Shen, K. Li, Y. Lv, T. Xu, D. Wei, Z. Liu, *Adv. Energy Mater.* **2020**, 10, 1904281.
- [10] a) J. Chang, J. Shang, Y. Sun, L. K. Ono, D. Wang, Z. Ma, Q. Huang, D. Chen, G. Liu, Y. Cui, Y. Qi, Z. Zheng, *Nat. Commun.* **2018**, 9, 4480; b) M. Yao, R. Wang, Z. Zhao, Y. Liu, Z. Niu, J. Chen, *ACS Nano* **2018**, 12, 12503; c) J.-H. Kim, Y.-H. Lee, S.-J. Cho, J.-G. Gwon, H.-J. Cho, M. Jang, S.-Y. Lee, S.-Y. Lee, *Energy Environ. Sci.* **2019**, 12, 177.
- [11] C. Jiang, L. Xiang, S. Miao, L. Shi, D. Xie, J. Yan, Z. Zheng, X. Zhang, Y. Tang, *Adv. Mater.* **2020**, 32, 1908470.

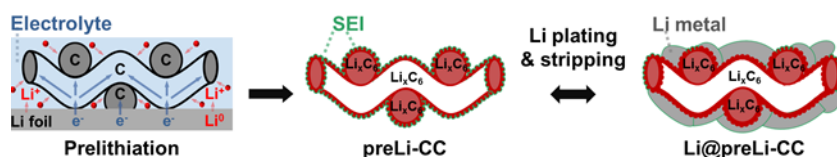
- [12] a) F. Mo, G. Liang, D. Wang, Z. Tang, H. Li, C. Zhi, *EcoMat* **2019**, 1, 12008; b) Y. Gao, H. Hu, J. Chang, Q. Huang, Q. Zhuang, P. Li, Z. Zheng, *Adv. Energy Mater.* **2021**, 11, 2101809; c) L. Wang, J. Shang, Q. Huang, H. Hu, Y. Zhang, C. Xie, Y. Luo, Y. Gao, H. Wang, Z. Zheng, *Adv. Mater.* **2021**, 33, 2102802; d) J. Xia, W. Chen, Y. Yang, X. Guan, T. Yang, M. Xiao, S. Zhang, Y. Xing, X. Lu, G. Zhou, *EcoMat* **2022**, DOI: 10.1002/eom2.12183e12183.
- [13] a) J. Chang, Q. Huang, Z. Zheng, *Joule* **2020**, 4, 1346; b) J. Chang, Q. Huang, Y. Gao, Z. Zheng, *Adv. Mater.* **2021**, 33, 2004419.
- [14] a) J. R. Dahn, J. C. Burns, D. A. Stevens, *Electrochem. Soc. Interface* **2016**, DOI: 10.1149/2.F07163if; b) J. Xiao, Q. Li, Y. Bi, M. Cai, B. Dunn, T. Glossmann, J. Liu, T. Osaka, R. Sugiura, B. Wu, J. Yang, J.-G. Zhang, M. S. Whittingham, *Nat. Energy* **2020**, 5, 561.
- [15] a) J. D. McBrayer, M.-T. F. Rodrigues, M. C. Schulze, D. P. Abraham, C. A. Apblett, I. Bloom, G. M. Carroll, A. M. Colclasure, C. Fang, K. L. Harrison, G. Liu, S. D. Minter, N. R. Neale, G. M. Veith, C. S. Johnson, J. T. Vaughey, A. K. Burrell, B. Cunningham, *Nat. Energy* **2021**, 6, 866; b) G. M. Hobold, J. Lopez, R. Guo, N. Minafra, A. Banerjee, Y. Shirley Meng, Y. Shao-Horn, B. M. Gallant, *Nat. Energy* **2021**, 6, 951.
- [16] a) T. T. Zuo, X. W. Wu, C. P. Yang, Y. X. Yin, H. Ye, N. W. Li, Y. G. Guo, *Adv. Mater.* **2017**, 29, 1700389; b) R. Tian, H. Duan, Y. Guo, H. Li, H. Liu, *Small* **2018**, 14, 1802226; c) J. Chang, H. Hu, J. Shang, R. Fang, D. Shou, C. Xie, Y. Gao, Y. Yang, Q. N. Zhuang, X. Lu, Y. K. Zhang, F. Li, Z. Zheng, *Small* **2022**, 18, e2105308; d) Y. Gao, Q. Guo, Q. Zhang, Y. Cui, Z. Zheng, *Adv. Energy Mater.* **2020**, 11, 2002580.
- [17] a) Y. Sun, G. Zheng, Zhi W. Seh, N. Liu, S. Wang, J. Sun, Hye R. Lee, Y. Cui, *Chem* **2016**, 1, 287; b) C. Martin, M. Genovese, A. J. Louli, R. Weber, J. R. Dahn, *Joule* **2020**, 4, 1296; c) Y. Son, T. Lee, B. Wen, J. Ma, C. Jo, Y.-G. Cho, A. Boies, J. Cho, M. De Volder, *Energy Environ. Sci.* **2020**, 13, 3723; d) W. Cai, C. Yan, Y. X. Yao, L. Xu, X. R. Chen, J. Q. Huang, Q. Zhang, *Angew. Chem. Int. Ed. Engl.* **2021**, 60, 13007.
- [18] a) P. Shi, T. Li, R. Zhang, X. Shen, X. B. Cheng, R. Xu, J. Q. Huang, X. R. Chen, H.

- Liu, Q. Zhang, *Adv. Mater.* **2019**, 31, 1807131; b) J. Duan, Y. Zheng, W. Luo, W. Wu, T. Wang, Y. Xie, S. Li, J. Li, Y. Huang, *Natl. Sci. Rev.* **2020**, DOI: 10.1093/nsr/nwz222.
- [19] a) N. Liu, L. Hu, M. T. McDowell, A. Jackson, Y. Cui, *ACS Nano* **2011**, 5, 6487; b) R. Zhan, X. Wang, Z. Chen, Z. W. Seh, L. Wang, Y. Sun, *Adv. Energy Mater.* **2021**, 11, 2101565; c) X. Min, G. Xu, B. Xie, P. Guan, M. Sun, G. Cui, *Energy Storage Mater.* **2022**, 47, 297; d) F. Wang, B. Wang, J. Li, B. Wang, Y. Zhou, D. Wang, H. Liu, S. Dou, *ACS Nano* **2021**, 15, 2197.
- [20] A. Shellikeri, V. Watson, D. Adams, E. E. Kalu, J. A. Read, T. R. Jow, J. S. Zheng, J. P. Zheng, *J. Electrochem. Soc.* **2017**, 164, 3914.
- [21] R. L. Sacci, L. W. Gill, E. W. Hagaman, N. J. Dudney, *J. Power Sources* **2015**, 287, 253.
- [22] a) C. Zhang, Q. Lan, Y. Liu, J. Wu, H. Shao, H. Zhan, Y. Yang, *Electrochim. Acta* **2019**, 306, 407; b) Y. Gao, Z. Yan, J. L. Gray, X. He, D. Wang, T. Chen, Q. Huang, Y. C. Li, H. Wang, S. H. Kim, T. E. Mallouk, D. Wang, *Nat. Mater.* **2019**, 18, 384.
- [23] Y. Gu, W. W. Wang, Y. J. Li, Q. H. Wu, S. Tang, J. W. Yan, M. S. Zheng, D. Y. Wu, C. H. Fan, W. Q. Hu, Z. B. Chen, Y. Fang, Q. H. Zhang, Q. F. Dong, B. W. Mao, *Nat. Commun.* **2018**, 9, 1339.

In this work, a facile direct-contact prelithiation method is used for the fabrication of prelithiated carbon cloth (preLi-CC) and the as fabricated anode enables the assembly of flexible hybrid lithium-ion/metal batteries (f-LIMBs), which present both high ICE, long cycling stability, enhanced energy density as well as excellent flexibility compared to the conventional LIBs.

Chuan Xie, Jian Chang, Jian Shang, Lei Wang, Yuan Gao, Qiyao Huang, Zijian Zheng*

Title: Hybrid lithium-ion/metal electrodes enable long cycle stability and high energy density of flexible batteries



Supporting Information

Hybrid lithium-ion/metal electrodes enable long cycle stability and high energy density of flexible batteries

Chuan Xie, Jian Chang, Jian Shang, Lei Wang, Yuan Gao, Qiyao Huang, Zijian Zheng*

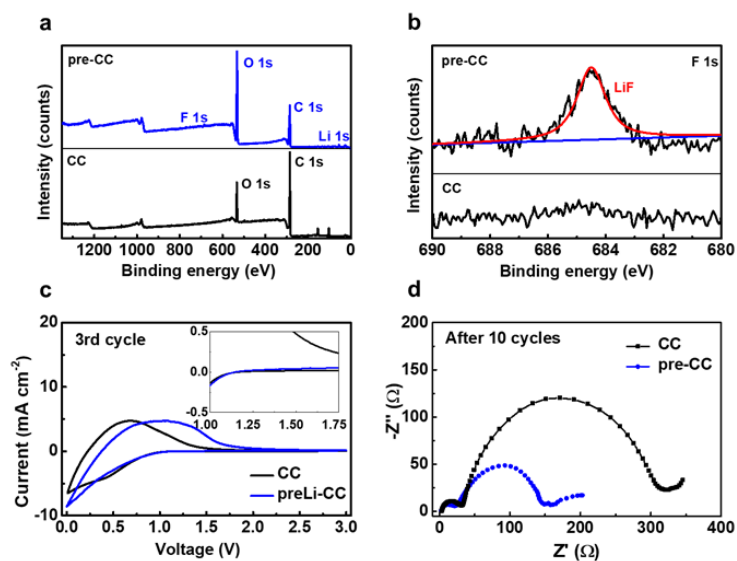


Figure S1. a) Full XPS spectrum of CC and preLi-CC. b) F 1s XPS spectrum of CC and preLi-CC. c) CV curves of the CC and preLi-CC electrode in the 3rd cycle. d) Impedance evolution of the CC electrode after 10 charge-discharge cycles.

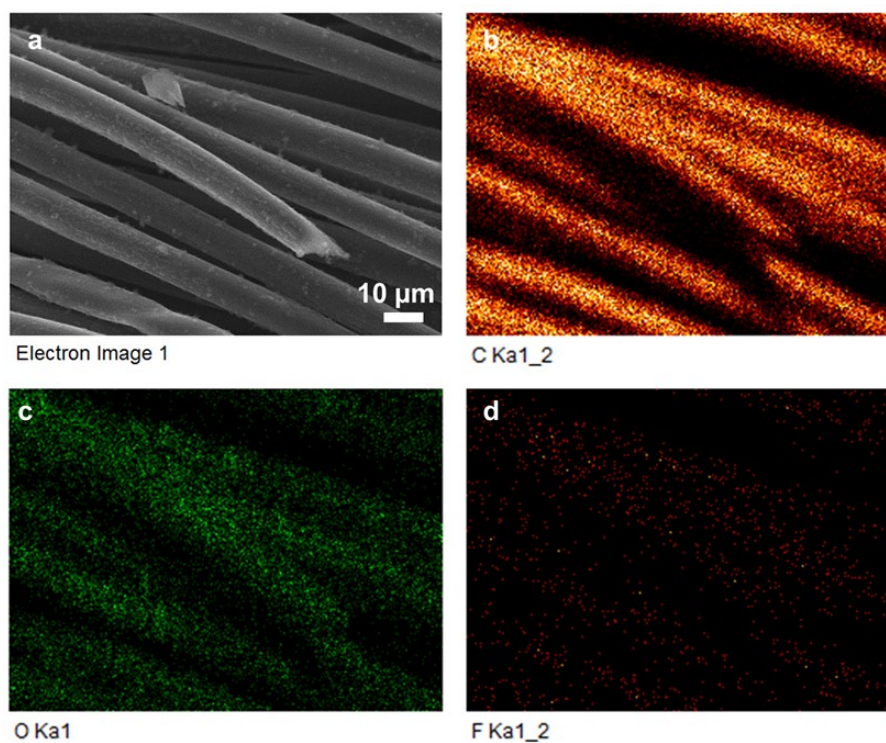


Figure S2. SEM image (a) and energy dispersive x-ray (EDX) mapping analysis of carbon (b), oxygen (c), and fluorine (d) of preLi-CC anode after stripping the Li^+ away.

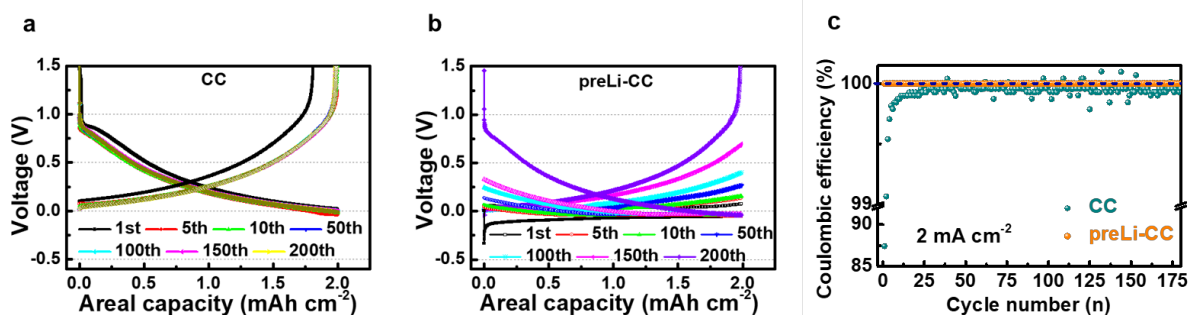


Figure S3. Charge/discharge evolution of the CC//Li half cell (a) and the preLi-CC//Li half cell (b). c) CEs of the CC and preLi-CC anode at a current density of 2 mA cm^{-2} .

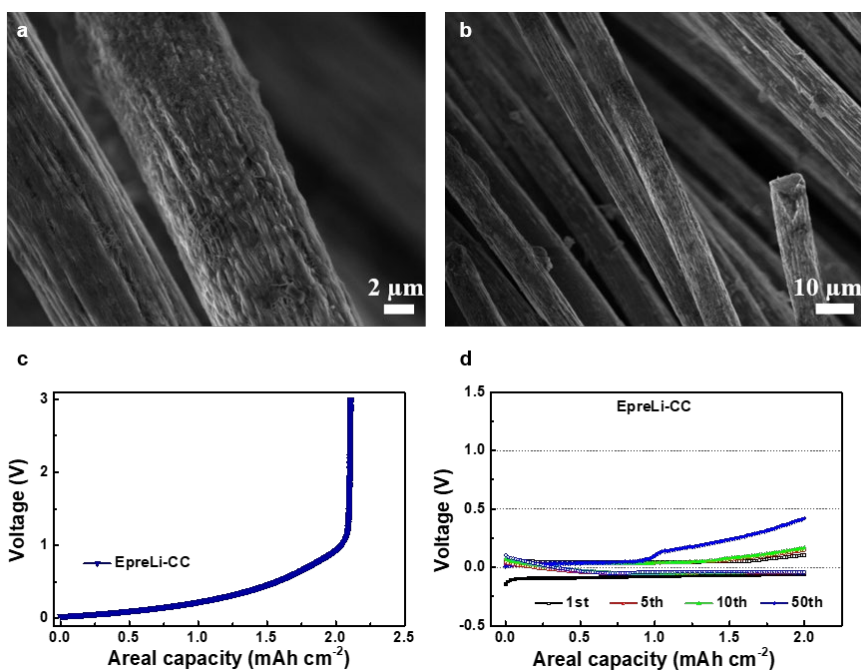


Figure S4. a-b). SEM images of the electrochemically prelithiated CC at high (a) and low (b) magnification. c). The stripped capacity of the EpreLi-CC at a current density of 0.25 mA cm^{-2} . d). Voltage profiles of the EpreLi-CC anode, showing a hybrid Li storage mechanism of Li-ion intercalation/de-intercalation and Li-metal plating/stripping.

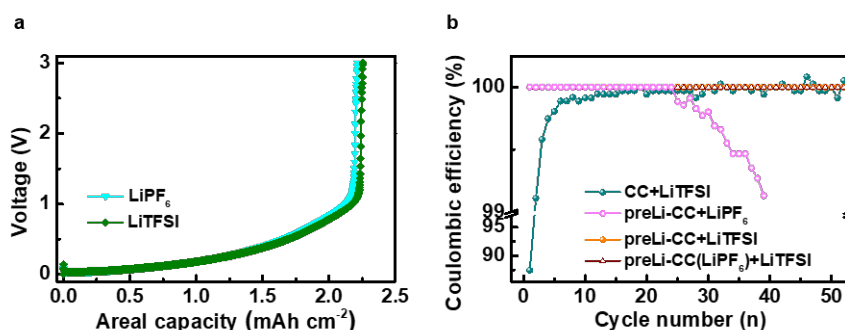


Figure S5. a). The stripped capacity of the preLi-CC prepared in LiTFSI-based and LiPF₆-based electrolyte at a current density of 0.25 mA cm^{-2} . The prelithiation time is 120 minutes. b). CE of the pristine CC cycling in LiTFSI-based electrolyte, preLi-CC cycling in LiPF₆-based and LiTFSI-based electrolyte, and preLi-CC prepared in LiPF₆-based electrolyte and cycling in LiTFSI-based electrolyte. The current density used here was 2 mA cm^{-2} .

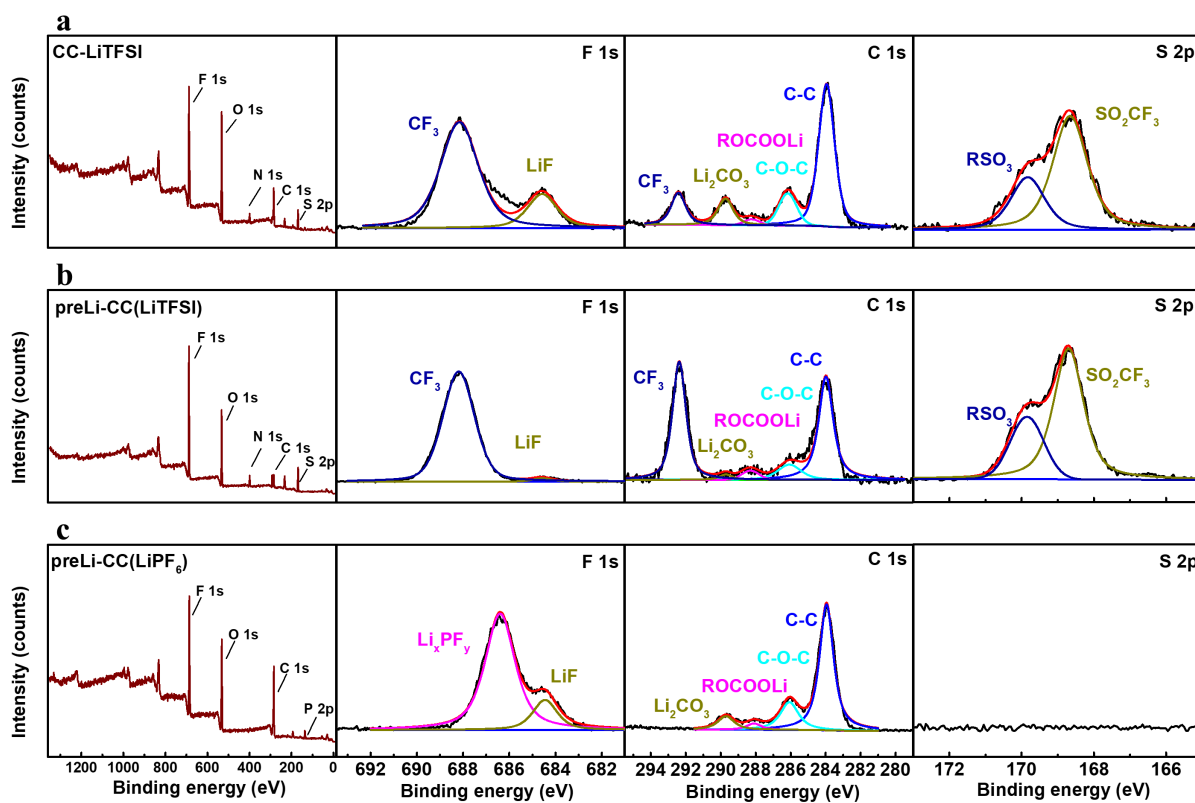


Figure S6. XPS spectrum of the CC-LiTFSI (a), preLi-CC (LiTFSI) (b), and preLi-CC (LiPF₆) (c) after 1st cycle.

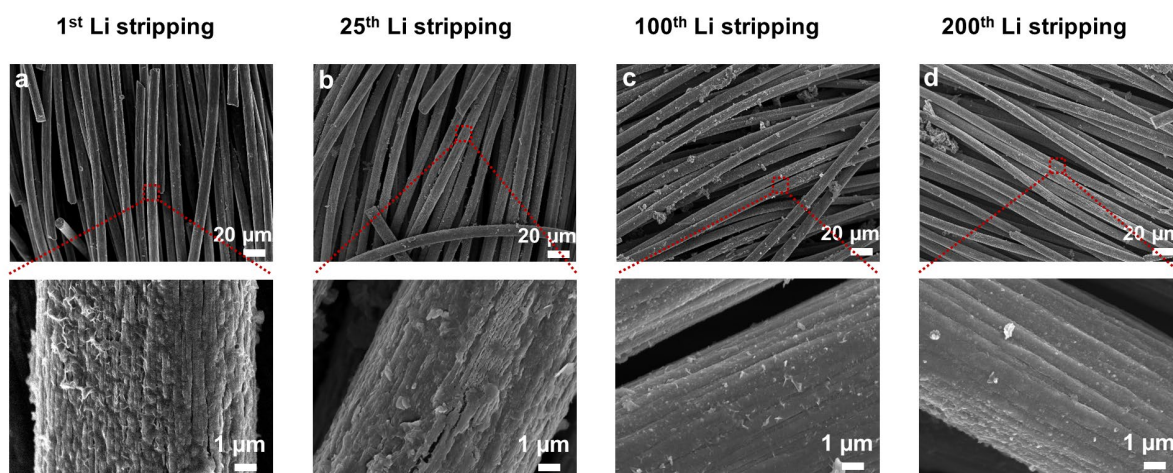


Figure S7. SEM images the preLi-CC electrodes after 1st (a), 25th (b), 100th (c), and 200th Li stripping (d).

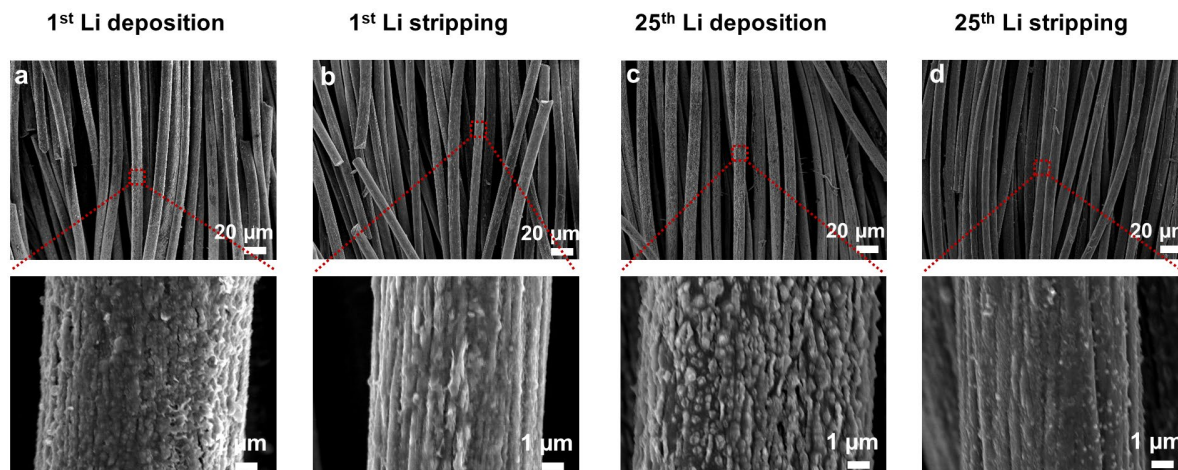


Figure S8. a-b) SEM images of the CC electrodes after 1st Li deposition (a) and stripping (b). c-d) SEM images of the CC electrode after 25th Li deposition (c), and stripping (d).

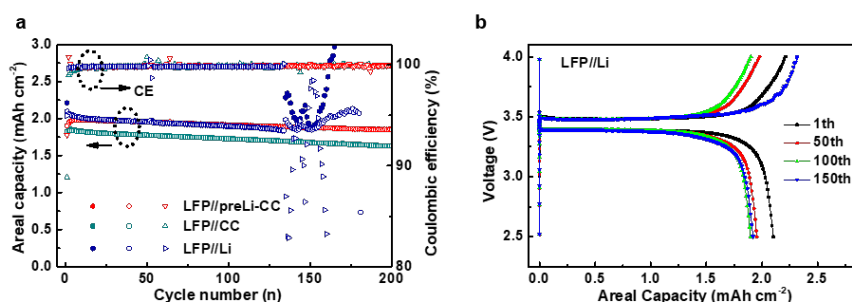


Figure S9. Cell performances of the preLi-CC, CC, and Li anodes paired with LFP. a) Cycling stability of the LFP//preLi-CC, LFP//CC, and LFP//Li. The cells were tested at a current density of 1 mA cm⁻² from 2.5-4 V for LFP//preLi-CC and LFP//Li, 1.5-4 V for LFP//CC. b) Charge/discharge profiles of the LFP//Li.

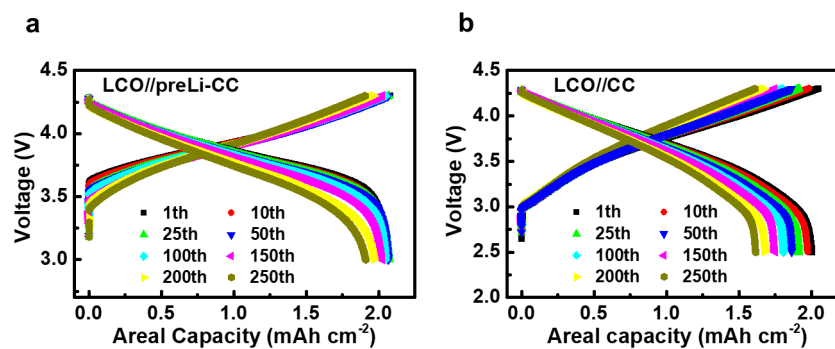


Figure S10. a) The charge/discharge curves of the LCO//preLi-CC full cell. b) The charge/discharge curves of the LCO//CC full cell.

Table S1. Comparison of our f-LIMBs with the state-of-the-art flexible lithium batteries.

Reported works	Anode	Energy density (mWh cm ⁻²)	Capacity retention (cycle number)	Flexibility	Reference
This work	Prelithiated carbon cloth	~6.8	84% (1000)	400 bending @ R=20, 10, 5, 2.5 mm	This work
Ref. 1	LTO/Non-woven fabric	~2.8	93.6% (450)	400 bending @ R=40, 30, 20, 10 mm	<i>Adv. Energy Mater.</i> 2015 , 5, 1401389.
Ref. 2	Si/CNT/PAN nanocomposite	~3.9	76% (100)	100 bending @ R= 5 mm	<i>Adv. Energy Mater.</i> 2017 , 7, 1701099.
Ref. 3	Li/Cu-Carbon fabric	~6.3	71.4% (260)	200 bending @ R= 5 mm	<i>Nat. Commun.</i> 2018 , 9, 4480.
Ref. 4	LTO/Carbon fabric	~2.1	94.6% (100)	100 bending @ R= 10 mm	<i>Small</i> 2018 , 14, 1703418.
Ref. 5	NiCo ₂ O ₄ /Carbon cloth	~3.5	78.9% (150)	200 folding	<i>Energy Environ. Sci.</i> 2018 , 11, 1859.
Ref.6	Graphite/NiCu-PET	~5.6	80.6% (90)	>1000 folding	<i>Small</i> 2018 , 14, e1703028.
Ref. 7	Li/PET	~5.67	65% (500)	1000 bending @ R= 2.5 mm	<i>Energy Environ. Sci.</i> 2019 , 12, 177.
Ref. 8	LTO/Graphene	~3.19	98.1% (100)	>100000 bending @ R= 10 mm	<i>Adv. Energy Mater.</i> 2020 , 10, 1904281.
Ref. 9	Li/Carbon cloth	~6.2	95% (560)	500 bending @ R=10mm	<i>Small</i> 2022 , 18, e2105308.
Ref. 10	Li/Carbon cloth	~10.5	60% (800)	Bent @ $\theta = 90^\circ$	<i>ACS Nano</i> 2021 , 15, 1358.